Colloids and Surfaces A: Physicochem. Eng. Aspects 481 (2015) 633–643

Contents lists available at ScienceDirect

Colloids and Surfaces A: Physicochemical and Engineering Aspects

journal homepage: www.elsevier.com/locate/colsurfa

Relaxation oscillations of solutal Marangoni convection at curved interfaces

K. Schwarzenberger[a], S. Aland[b], H. Domnick[a], S. Odenbach[a], K. Eckert[a,*]

[a] Institute of Fluid Mechanics, Chair of Magnetofluiddynamics, Measuring and Automation Technology, TU Dresden, 01062 Dresden, Germany
[b] Institute of Scientific Computing, TU Dresden, 01062 Dresden, Germany

HIGHLIGHTS

- Relaxation oscillations were observed in a simple 2-phase mass-transfer system.
- They are caused by repeated consumption and regeneration of Marangoni driving force.
- Interfacial curvature affects the appearance of relaxation oscillations.
- Numerous regular cycles occur at drops or bubbles.
- Simulations at drops and bubbles reproduce the relaxation oscillations.

GRAPHICAL ABSTRACT

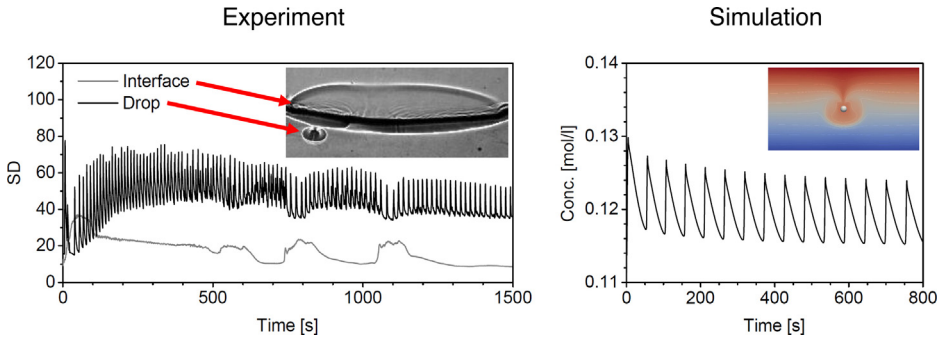

ARTICLE INFO

Article history:
Received 30 April 2015
Received in revised form 13 June 2015
Accepted 16 June 2015
Available online 21 June 2015

Keywords:
Solutal Marangoni convection
Relaxation oscillations
Interfacial curvature
Hele-Shaw model
Phase-field simulations

ABSTRACT

Relaxation oscillations in a two-phase system, consisting of paraffin oil and water, with 2-propanol initially dissolved in the oil phase, are observed as a periodic decay and re-amplification of interfacial convection. Due to the mass transfer of the weakly surface-active 2-propanol, concentration gradients and, by implication, density gradients exist. This leads to a periodic coupling of Marangoni instability, buoyant convection and the restoring effects of diffusion. The relaxation oscillations are facilitated by the presence of interfacial curvature, which imposes additional gradients of interfacial tension. This effect is particularly pronounced around drops or bubbles formed in the experiments. The markedly regular relaxation oscillations appearing in that case have been further studied by 2D Hele-Shaw simulations based on a diffuse-interface model. Interfacial tension is assumed to depend linearly on 2-propanol concentration without accumulation of matter at the interface. This simplified approach is capable of reproducing the relaxation oscillations observed experimentally.

1. Introduction

Interfacial-tension driven flow, known as Marangoni convection, takes place in various technological processes such as extraction, evaporation or absorption of exhaust gas components. It originates from gradients in the temperature (thermocapillary case) or concentration of a surface-active substance (solutocapillary case). Even if the magnitude of Marangoni convection decreases rapidly with the distance from the interface, it changes the heat and mass transfer rates observed in such systems. This effect, already noted in the early experiments of Sherwood and Wei [1], motivated continuing research on Marangoni flow structures

* Corresponding author.
E-mail address: Kerstin.Eckert@tu-dresden.de (K. Eckert).

http://dx.doi.org/10.1016/j.colsurfa.2015.06.031
0927-7757/

and their relation to mass transfer efficiency [2–5]. Furthermore, new technologies are developed which use these flow structures to pattern functional surfaces [6,7].

The first theoretical approach to predict the onset of solutal Marangoni instability was accomplished by Sternling and Scriven [8], who considered mass transfer of a weakly surface-active solute between two liquid layers separated by a planar interface. Their linear stability analysis confirmed the intuitive expectation that small perturbations are amplified to stationary roll cell convection if the solute diffuses out of the layer with higher kinematic viscosity and lower solute diffusivity (cf. Section 2.1). Subsequent studies further extended their linear stability analysis, e.g. to interfacial deformations [9], the influence of adsorption kinetics [10], or to the effects of solvent diffusion [11].

However, in contrast to the simple roll cells predicted by the linear theory, solutal Marangoni convection mostly shows complex and unsteady flow patterns, cf. the overview given in [12]. The combination of experimental flow visualization and numerical analysis has recently improved understanding of the mechanisms underlying the evolution of patterns in Marangoni convection [13–15]. According to [15], a typical feature is the coarsening of structures, i.e. a steady increase in the size of the Marangoni cells, which compensates for the equilibrated mixing zone inside the cells by entraining fresh fluid. Besides this continuous process, some systems show a temporal periodicity in Marangoni convection. This evolution is characterized by subsequent decays and re-amplifications of large-scale Marangoni structures. Even simple mass transfer systems with a weakly surface-active solute can feature such a temporal periodicity [16,17,12]. The decay of convection is attributed to the self-induced consumption of driving concentration gradients by enhanced mass transfer and the mixing effect of Marangoni structures in the vicinity of the interface [12]. A stable density stratification is required for the build-up of this equilibrated zone since otherwise buoyant convection would provide a constant supply of fresh fluid from the bulk phases [17]. For the same reason, the coarsening mechanism must be prevented, e.g. by geometrical confinement of the structures in the horizontal direction or by a strong density stratification that limits the vertical length scale.

Particularly pronounced periodicity develops in systems with mass transfer of a strong surfactant. This was observed by time-dependent interfacial tension measurements [18–20] or visualization of the flow patterns [21,18]. Again, two phases of varying convective intensity occur repeatedly. In the phase of active Marangoni convection, the enhanced supply of surfactant causes a rapid drop in interfacial tension, whereas a slow rise in interfacial tension is observed for the ensuing phase of weak convection. A similar characteristic is obtained by the spreading of a surfactant from a point-like source located under a surface or an interface [22,23]. Here, a single convection cell periodically decays and rekindles due to the combined action of adsorption–desorption kinetics and geometric confinement. Additional buoyancy effects in such systems alter the appearance of the oscillations, but are not their origin [24].

Depending on the configuration, the buoyancy influence can play different roles. In [25,26], an initially stable density stratification is provided for a bubble or a drop placed in an aqueous surfactant solution with a vertical concentration gradient. The spreading of the surfactant by Marangoni convection causes buoyancy-driven convection. The interaction between both effects again gives rise to an oscillatory flow. On the other hand, unsteady Marangoni convection can also be provoked by a primary buoyancy instability, e.g. for a drop of partially miscible fluid dissolving in a surrounding liquid with an imposed vertical temperature gradient [27]. Furthermore, buoyancy instability can trigger interfacial tension-driven spreading for mass transfer in the Marangoni-stable direction [28]. The situation becomes even more complex if Marangoni effects are coupled to chemical reactions. In fact, oscillations can be observed for a variety of reactive systems [29–35]. Additional effects like chemical interaction of the solutes in the interfacial region, multi-component diffusion of educts and products or phase changes like precipitation however require a specific interpretation for each system.

Despite their diversity, all of the systems listed above show a similar characteristic in their temporal evolution. Impulsive stages of active Marangoni convection alternate with longer relaxation periods during which the Marangoni driving force is restored. This typical progression, termed relaxation oscillations, results from the different time scales of Marangoni convection compared to concurrent processes like diffusion or other types of convection.

In this work, we show that relaxation oscillations set in even when a common alcohol is employed instead of a strong surfactant or a chemical reaction. For the first time, the temporal periodicity of such a simple mass transfer system is analyzed in detail. A novel combination of experiments using drops and bubbles placed in a vertical alcohol concentration gradient with phase-field simulations allows us to unravel the oscillation mechanism: Intense mixing by the Marangoni convection locally cancels the driving concentration gradient. Restoration of the latter by buoyancy-driven convection and diffusion initiates the next oscillation period. The droplets represent the smallest length scale employed in our systematic variation of geometrical constraints and interfacial curvature. These insights are therefore valuable to understand why Marangoni convection breaks down at an extended interface and how the curvature of the interface supports re-amplification.

2. Experiment

2.1. Mass transfer system

We consider the two-layer system paraffin oil/water with mass transfer of 2-propanol. Initially, 5 vol% 2-propanol is dissolved in the upper organic phase which diffuses to the lower aqueous phase, see Fig. 1. 2-propanol lowers interfacial tension and the density of both the aqueous (1) and the organic phase (2). Since diffusivity is lower and kinematic viscosity is higher in the donating phase ($D^{(2)}/D^{(1)} < 1$, $\nu^{(2)}/\nu^{(1)} > 1$), diffusion of 2-propanol across the interface is prone to stationary Marangoni instability according to [8]. This can be illustrated by considering a small perturbation at the interface with a slightly higher solute concentration. As a result, a divergent motion of the interface will be initiated due to the Marangoni effect, advecting solute-rich fluid from the donating phase. Since the vertical concentration gradient in this phase is steeper on account of the lower solute diffusivity, this cannot be canceled out by the inflow of fluid poor in solute from the accepting phase. Hence the flow is amplified and Marangoni instability sets in.

Due to the hydrophilic nature of the short-chain alcohol, partition is largely in favour of the aqueous phase. This leads to an intense mass transfer and, accordingly, a fast depletion of the organic phase in regions near the interface. Besides, a stable density stratification is built up in both layers during the mass transfer. The corresponding material parameters, presented in Table 1, are taken from the literature [36,37] or estimated by suitable relationships as detailed in the following.

For the dependence of interfacial tension σ and solution density $\rho^{(i)}$ of phase $i = 1, 2$ on 2-propanol concentration $c^{(i)}$, a linear relation is assumed

$$\rho^{(i)} = \rho^{(i)}_{ref} + \rho^{(i)}_{ref}\beta^{(i)}_c c^{(i)}, \tag{1}$$

$$\sigma = \sigma_{ref} + \sigma_{ref}\alpha_c c^{(1)}. \tag{2}$$

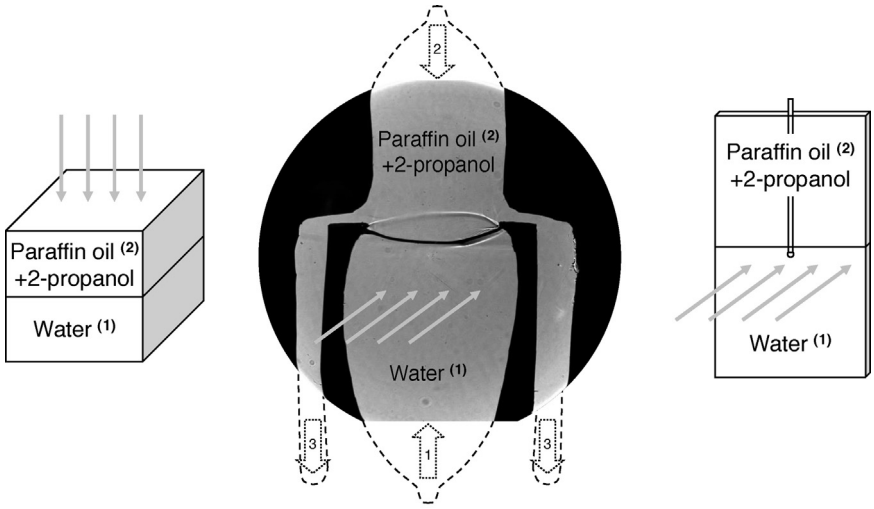

(a) Cubic cuvettes (b) Hele-Shaw cell (c) Capillary

Fig. 1. Experimental setups to study Marangoni convection in the system paraffin oil/water with interfacial mass transfer of 2-propanol. Light gray arrows indicate the direction of observation in the shadowgraph optics. Numbered block arrows in (b) mark the inlet and outlet of liquids during the filling procedure in the Hele-Shaw cell as detailed in the text.

The solutal expansion coefficient $\beta_c^{(i)}$ was obtained by linear interpolation between the densities of the pure phases $\rho_{ref}^{(i)}$ and the density of the pure solute ρ_p, i.e. neglecting excess volume of mixing.

The interfacial tension of the binary system σ_{ref} and the change of interfacial tension with solute concentration $\sigma_{ref}\alpha_c$ is approximated by measurements of the system hexane/water/2-propanol [38]. The equilibrium data of this ternary system is also listed in [38] and used to calculate the partition coefficient $H = c_{eq}^{(2)}/c_{eq}^{(1)}$, where $c_{eq}^{(i)}$ are the molar concentrations at partition equilibrium. The approximation with the aid of hexane is motivated by the similar chemical nature of paraffin oil which is a mixture of alkanes with longer carbon chains. However, viscosity $\eta^{(2)}$ and diffusivity $D^{(2)}$ strongly depend on the chain length of the alkane molecules. For liquid paraffin, a typical range of 16–32 carbon groups is reported in literature [41]. The paraffin oil of lower viscosity used in this study probably contains more of the shorter chains, so that a mean chain length of 20 carbon groups is assumed for the molar mass $M^{(2)}$ in Table 1. On this basis, the diffusivity of 2-propanol in paraffin oil $D^{(2)}$ is calculated using the Wilke and Chang correlation [40]. A deviation in chain length of ±4 carbon groups would amount to 10% uncertainty in the diffusion coefficient; hence, this estimation is robust on its order of magnitude.

All chemical substances were used as purchased. Water and 2-propanol were of HPLC grade, and the paraffin oil was of pharmaceutical quality (Ph.Eur., DAB). In preliminary experiments, however, the system turned out to be very sensitive to impurities, resulting in strongly reduced or even inhibited Marangoni convection for contaminated experimental runs. Therefore, in this study, a rigorous cleaning procedure was undertaken. All relevant equipment and experimental containers were flushed and wiped with acetone, then triply rinsed both with distilled water and 99% ethanol.

An advantage of this mass transfer system – besides the harmless chemical substances – is the negligible mutual solubility of the

Table 1
Properties of the system paraffin oil/water with interfacial mass transfer of 2-propanol at room temperature. Phase 1 is the aqueous phase marked with upper index (1) and phase 2 the organic phase marked with (2). The data sources are further detailed in the text.

Description	Symbol	Unit	Value	Ref.
Molar mass water	$M^{(1)}$	kg/mol	18.02×10^{-3}	[36]
Molar mass paraffin oil (eicosane)	$M^{(2)}$	kg/mol	282.55×10^{-3}	[36]
Molar mass 2-propanol	M_p	kg/mol	60.10×10^{-3}	[36]
Mass density water	$\rho_{ref}^{(1)}$	kg/m^3	998	[36]
Mass density paraffin oil	$\rho_{ref}^{(2)}$	kg/m^3	850	[37]
Mass density 2-propanol	ρ_p	kg/m^3	781	[36]
Dynamic viscosity water	$\eta^{(1)}$	Pa s	1.00×10^{-3}	[36]
Dynamic viscosity paraffin oil	$\eta^{(2)} = \nu^{(2)}\rho_{ref}^{(2)}$	Pa s	28.9×10^{-3}	
Kinematic viscosity water	$\nu^{(1)} = \eta^{(1)}/\rho_{ref}^{(1)}$	m^2/s	1.00×10^{-6}	
Kinematic viscosity paraffin oil	$\nu^{(2)}$	m^2/s	34×10^{-6}	[37]
Partition coefficient	H	(mol/l)/(mol/l)	0.16	[38]
Diffusivity 2-propanol in water	$D^{(1)}$	m^2/s	1.08×10^{-9}	[39]
Diffusivity 2-propanol in paraffin oil	$D^{(2)}$	m^2/s	9×10^{-11}	[40]
Interfacial tension of the binary system	σ_{ref}	N/m	50.1×10^{-3}	[38]
Change of interfacial tension per 2-propanol conc. in water	$\sigma_{ref}\alpha_c$	N/m/(mol/l)	−0.136	[38]
Solutal expansion coefficient 2-propanol in water	$\beta_c^{(1)}$	l/mol	−0.0167	
Solutal expansion coefficient 2-propanol in paraffin oil	$\beta_c^{(2)}$	l/mol	−0.0062	
Initial conc. for 5 vol% 2-propanol	c_0	mol/l	0.649	
Gravitational acceleration	g	m/s^2	9.81	

basic phases, paraffin oil and water, so that no presaturation of both solvents is required. Corresponding to the low solubility, interfacial tension between paraffin oil and water is high. This property determines not only the strong adsorption of impurities [42] as described above, but also the shape of the interface, cf. Section 3.

In addition to the system paraffin oil/water/2-propanol, relaxation oscillations at an air bubble placed in the aqueous phase are shown in Sections 3 and 4.2. Table 2 summarizes the material parameters that describe Marangoni convection at the bubble surface along with the corresponding references. As done for the interfacial tension dependence $\sigma_{ref}\alpha_c$, a linear relation is assumed for the change of surface tension with solute concentration in the aqueous phase, $\gamma_{ref}\alpha_c^*$. Since mass transfer into the bubble is neglected (see Section 4.1), only the density ρ_{air} and the viscosity η_{air} of the air phase are needed.

2.2. Experimental setup

The system geometry is an important factor for the onset of temporal periodicity in Marangoni convection (cf. Section 1), as it limits the accessible volume of fresh fluid required to maintain the coarsening of the convective structures. Therefore, in this study, we conduct a systematic variation of geometry. First, the system of Section 2.1 is placed in rectangular cuvettes of different side lengths. Second, the geometry is further restricted by using a capillary gap, the Hele-Shaw cell. This additionally allows us to control the curvature of the interface as detailed below. Third, drops and bubbles formed inside the system of Section 2.1 are analyzed; these set the smallest length scale imposed. The experiments in the cuvettes provide a top view at the interface, whereas in the Hele-Shaw cell, the flow structures are observed normal to the interface. A shadowgraph optics (construction by TSO, Pulsnitz, Germany), detecting the second derivative of the concentration field, is applied to visualize the patterns arising from interfacial convection. Fig. 1 schematically illustrates the different experimental geometries.

Two different cuvette aspect ratios are used to check if the appearance of temporal periodicity is robust for a certain variation of geometry: cubic cuvettes with inner dimensions of $L \times W \times H = 20\,\text{mm} \times 20\,\text{mm} \times 20\,\text{mm}$ as shown in Fig. 1(a) and narrow cuvettes with $L \times W \times H = 60\,\text{mm} \times 10\,\text{mm} \times 20\,\text{mm}$. Due to the high interfacial tension of the basic phases paraffin oil and water, the liquids can be superposed by cautiously pouring the organic phase over the aqueous one using a syringe. The cuvettes are filled to the brim and then covered with a glass plate to prevent evaporation of 2-propanol.

Fig. 1(b) depicts a shadowgraph image of the Hele-Shaw cell filled with the system (paraffin oil + 2-propanol)/water in a typical state of the mass transfer experiment. Two parallel glass plates form the narrow gap of the Hele-Shaw cell. A spacer made of polytetrafluoroethylene (PTFE) foil, whose inner contour is further sketched by a dashed line beyond the circular field of view, sets the gap width $d = 1\,\text{mm}$, see Section 4.1. The shape of the PTFE foil and the filling procedure are adapted from [44–46]. The numbered arrows in Fig. 1(b) mark the inlet and outlet of liquids during the filling procedure. First the aqueous phase is injected from the bottom inlet (1) until the Hele-Shaw cell is completely filled with liquid. Next, the organic phase is filled from the top inlet (2) until it occupies the upper half of the Hele-Shaw cell. To obtain a defined starting condition, the organic and aqueous phase then are continuously fed from above and below until the interface is refreshed. Finally, injection of the aqueous phase is stopped, so that the organic phase completely fills the exhaust channels (3). During this step, the interface (visible as a thick black line separating the two phases in Fig. 1(b)) pins at the lateral edges of the PTFE foil. The distance between these edges amounts to 15 mm. By the pinning effect, it is possible to obtain a planar (Fig. 4(c)) or even concave[1] (Fig. 4(a)) form of the interface. Without pinning, the interface assumes a convex shape due to the wetting of the hydrophobic PTFE foil by the organic phase as visible in Fig. 4(b). At the end of the filling procedure, the desired shape of the interface can be further tuned by a cautious injection or suction of a small amount of liquid from above or below.

Finally, drops sitting on the glass wall of the Hele-Shaw cell are examined; these formed incidentally during the filling procedure in some experiments. The diameter of the drops is typically 0.1–0.5 mm, corresponding to a volume of a few nanoliters. In addition, air bubbles are introduced in further experiments via a capillary as depicted in Fig. 1(c). In that case, a larger Hele-Shaw gap width of 3 mm is used so that the capillary can be inserted.

3. Experimental results

3.1. Cuvettes

To provide an overview on the evolution in the system (paraffin oil + 2-propanol)/water, Fig. 2 shows characteristic stages of Marangoni convection for the cubic cuvettes. After the superposition of the phases, a large-scale Marangoni flow develops, visible as high-contrast concentration fronts occupying the whole cuvette cross-section in Fig. 2(a). Simultaneously, small structures appear at the interface in the form of high-frequency modulations of gray value. This hierarchy of large-scale convection with an embedded substructure is a common feature of solutal Marangoni instability and was analyzed in-depth in [15]. The ensuing relaxation phase in Fig. 2(b) is marked by weak convection with faint structures at the interface until the next active phase (c) sets in.

The difference in contrast between active and relaxation phase is visualized by the gray value distribution in Fig. 3(a). Intense concentration fronts in the active phase result in a broad distribution, whereas the relaxation phase features a narrow peak around the mean gray value. Hence, the standard deviation (SD) of the gray value distribution can be used as a measure to characterize the intensity of convection. The change in standard deviation with time readily describes the re-amplifications of Marangoni convection, see Fig. 3(b). This diagram shows the temporal evolution for both the cubic cuvette and the narrow cuvette. In the cubic cuvette (upper graph), three short peaks of intense convection can be observed. Beyond $t = 3000\,\text{s}$, the driving force is no longer sufficient to drive another cycle of large-scale Marangoni convection. For the narrow cuvette, the smallest dimension of the interface is 10 mm, and the largest one is 60 mm. Accordingly, the length scale of convective structures is even more confined in the lateral direction compared to the 20 mm × 20 mm interface in the cubic cuvettes. However, a larger reservoir of liquids is available at the same time. The temporal evolution in the narrow cuvette (lower graph in Fig. 3(b)) therefore exhibits longer active phases and its last re-amplification occurs at a later time (peak at $t = 6000\,\text{s}$).

Apart from the change in gray value contrast, Fig. 2 reveals another feature of our liquid–liquid system. Regions close to the cuvette walls are shadowed by the deflection of light at the curved interface. The aqueous phase preferably wets the cuvette glass, thus a concave meniscus is formed. The characteristic size of the meniscus under gravity is represented by the capillary length $\kappa = \sqrt{\sigma/(g\Delta\rho)}$ [47]. A value of approx. 6 mm is obtained for the system paraffin oil/water with an interfacial tension of $\sigma_{ref} = 50 \times 10^{-3}\,\text{N/m}$ and a density difference $\Delta\rho_{ref} = 150\,\text{kg/m}^3$. Hence the size of the

[1] Considering a point at the interface, we construct a circle whose circular arc best approximates the shape of the interface at that point. If the center of this circle is located in the organic [aqueous] phase, we denote the interfacial curvature as concave [convex].

Table 2
Properties of the system air/(water + 2-propanol) at room temperature. The data sources are further detailed in the text.

Description	Symbol	Unit	Value	Ref.
Density air	ρ_{air}	kg/m^3	1.161	[36]
Dynamic viscosity air	η_{air}	Pa s	1.86×10^{-5}	[36]
Kinematic viscosity air	$\nu_{air} = \eta_{air}/\rho_{air}$	m^2/s	1.6×10^{-5}	
Surface tension of water	γ_{ref}	N/m	72.01×10^{-3}	[43]
Change in surface tension per 2-propanol conc. in water	$\gamma_{ref}\alpha_c^*$	N/m/(mol/l)	−0.0274	[43]

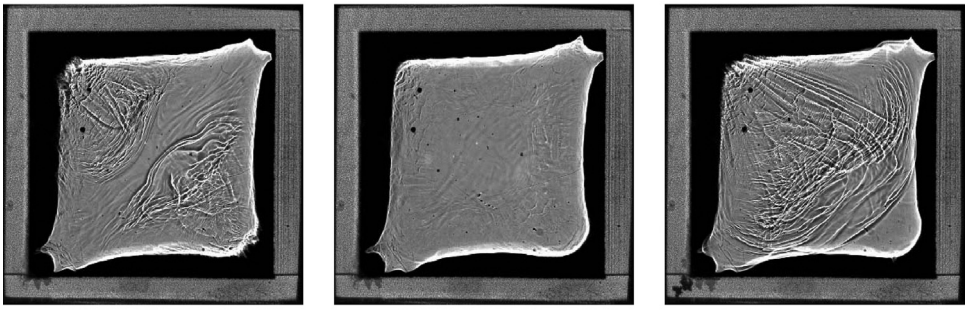

(a) Active phase at t = 390 s (b) Relaxation phase at t = 620 s (c) Active phase at t = 870 s

Fig. 2. Temporal evolution of Marangoni convection in the cubic cuvette for the system (paraffin oil + 5 vol% 2-propanol)/water. The size of the shown window is 25 mm × 25 mm.

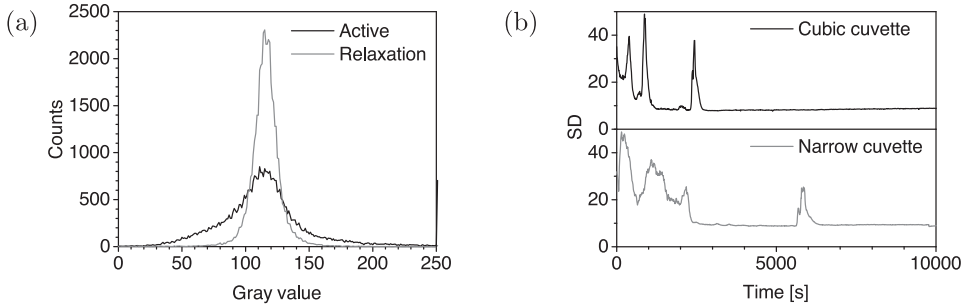

(a) Gray value distribution for active phase (t = 390 s) and relaxation phase (t = 620 s)

(b) Temporal evolution of standard deviation of gray values

Fig. 3. Evaluation of gray value distribution for repeated amplification of Marangoni convection in the cuvettes.

meniscus is not negligible with respect to the characteristic length of the system geometry (cuvette width of 20 mm). The slightly asymmetric shape of the interface, visible through the shadowed regions of Fig. 2, is caused by the filling procedure. The inflow points of Marangoni convection preferably are located at the highest positions of the concave meniscus, e.g. in the upper-left and lower-right corner of Fig. 2(a). Since the shape of the interface obviously influences the characteristics of Marangoni convection, this effect is further investigated in the Hele-Shaw cell.

3.2. Hele-Shaw cell

In the Hele-Shaw cell, the interface possesses two principal curvatures. Due to the hydrophilic glasses, which are preferably wetted by the aqueous phase, a concave curvature also exists in the small gap. As shown below, this curvature does not play a crucial role and therefore is of minor interest. More importantly, the second principal curvature can be tuned from concave to planar to convex simply by the volume injected of the respective phase (cf. Section 2.2). Fig. 4 shows shadowgraphs of the Marangoni convection developing for these three cases. The concave interface in Fig. 4(a) maps the situation in the cuvettes of Section 3.1. The inflow of solute-rich fluid (homogeneous gray value) from the organic bulk phase to the interface takes place at the lateral edges of the interface in Fig. 4(a), i.e. at the highest position of the interface. Accordingly, the inflow is located in the center of the interface for the convex case in Fig. 4(b). The fluid, mixed by the roll cell convection, again accumulates in the outflow zones. These regions of mixed fluid are separated from the organic bulk phase by a high-contrast concentration front arching over the center of the interface in Fig. 4(a) and the lateral sides in (b), respectively.

In [17,48], the influence of small deformations of an ideally planar interface was already briefly discussed. However this effect becomes particularly clear in Fig. 4((a) and (b)) by deliberately imposing a strong variation of curvature. Regions of the interface reaching farther into the upper donating phase, such as the edges (Fig. 4(a)) or the central part (Fig. 4(b)), are subjected to a higher concentration of surface-active solute. The resulting gradients in interfacial tension induce Marangoni convection towards regions of the interface penetrating into the accepting aqueous phase. Accordingly, a reverse flow direction appears for the concave and the convex case as marked by white arrows in Fig. 4((a) and (b)).

The variation in interfacial curvature not only affects the shape of Marangoni convection, but also its temporal evolution, see Fig. 5. After an intense initial phase, clear re-amplifications of Marangoni convection can only be observed for the concave (dark gray curve)

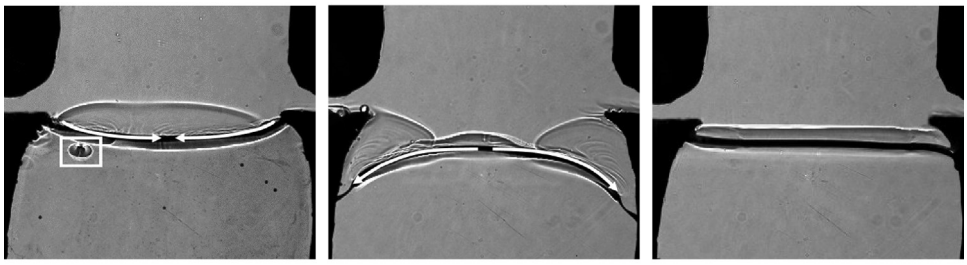

(a) Concave interface (b) Convex interface (c) Approx. planar interface

Fig. 4. Marangoni convection in the Hele-Shaw cell for varied interfacial curvature at $t = 100$ s. The interface is visible as a thick black line separating the upper organic from the lower aqueous phase. The width of the shown window is 20.7 mm. White arrows in (a) and (b) indicate the main direction of flow at the interface. The white rectangle in (a) marks a drop, later on referred to as Drop 1, with periodic Marangoni convection, see Section 3.3.

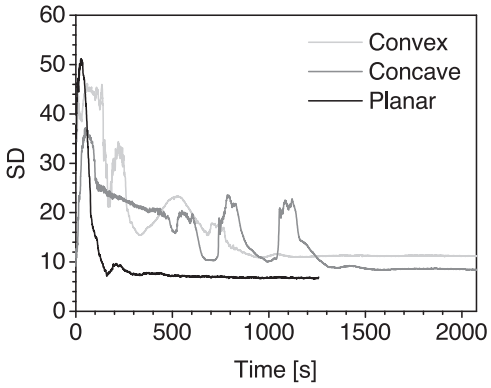

Fig. 5. Temporal evolution of standard deviation of gray value distribution in the Hele-Shaw cell for varied interfacial curvature.

and convex (light gray curve) cases. By contrast, at the planar interface (black curve) where the vanishing interfacial curvature along the glass walls does not impose a preferred flow direction (see Fig. 4(c)), the activity soon decays. We remark that a small convection also results from the curvature of the interface between the glass plates. Since it does not significantly influence the temporal evolution in Fig. 5, it deserves no further consideration for the present problem.

3.3. Drops and bubbles

In several experiments, small drops or bubbles formed during the filling of the Hele-Shaw cell or cuvette which stuck to the walls of the experimental container. In Fig. 4(a) such a drop of paraffin oil immersed in the aqueous phase is marked by a white rectangle. If the distance between the drop and the interface of the two-layer system is small enough, periodic re-amplifications of Marangoni convection can be observed at the drop surface. Within one cycle of re-amplification, characteristic stages of convection are passed. These stages are depicted in Fig. 6 for "Drop 1" which is marked in Fig. 4(a). The cycle begins with the start-up of Marangoni convection in Fig. 6(a). Two small vortices form at either side of the drop and are amplified to the state depicted in Fig. 6(b), where the peak of Marangoni convection is reached. The flow obviously is caused by the conditions in the surrounding of the drop. Due to the mass transfer of 2-propanol across the overlying interface of the two-layer system, the drop is placed in a vertical concentration gradient. Hence it is subjected to high solute concentration at the upper side, implying both low interfacial tension σ and density $\rho^{(1)}$, and low concentration at the bottom, i.e. both higher σ and $\rho^{(1)}$. Therefore, Marangoni convection at the drop surface is directed downwards, entraining lighter fluid rich in solute to lower regions of higher density. The initially stably stratified aqueous phase is stirred, and the additional buoyancy accelerates the rise of the lighter fluid at some distance from the drop surface. As a result, an intense mixing of the fluid, visible in Fig. 6(b), takes place which exhausts the vertical concentration gradient in the vicinity of the drop and leads to the breakdown of Marangoni convection. In the subsequent relaxation phase (Fig. 6(c)), the initial concentration gradient is restored by both the buoyancy-driven convection, which carries the mixed fluid upwards, and diffusion. The end of the relaxation phase is shown in Fig. 6(d), followed by another cycle of Marangoni convection. A similar mechanism was already observed in [26] for other fluid combinations.

The intensity of Marangoni convection which disturbs the concentration gradient in the surrounding of the drop can again be characterized by the standard deviation of the gray value distribution, see Fig. 7. The inset zooms in on three periods of Drop 1, indicating the sawtooth-like progression of the observed relaxation oscillations. The steep rise in standard deviation corresponds to the short, impulsive stage of Marangoni convection. The relaxation phase lasts longer due to the slower processes of diffusion and buoyant convection being responsible for the restoration of the Marangoni driving force. The main diagram shows about hundred periods of regular relaxation oscillations over half an hour. As Drop 1 is located close to the interface of the two-layer system, its relaxation oscillations are influenced to a certain extent by the large-scale Marangoni convection. To illustrate this, the intensity of convection at the interface (already shown in Fig. 5, concave case) is plotted again for comparison in Fig. 7 (gray curve). It can be seen that during active Marangoni convection of the two-layer system, i.e. a rise of the gray curve, the frequency of the relaxation oscillations at Drop 1 decreases. Under this additional mixing, it will take longer until the concentration gradient at the drop for the onset of the next oscillation is available again.

Figs. 8 and 9 show that such relaxation oscillations were observed in several experiments in the system (paraffin oil + 2-propanol)/water. Besides Drop 1 (located on the left-hand side of Fig. 8(a)), other drops further away from the interface (right-hand side of Fig. 8(a)) perform relaxation oscillations as the concentration gradient of the two-layer system advances into the aqueous phase. Generally, the concentration gradient decreases with the distance from the interface. Accordingly, the contrast of the concentration fronts produced by the Marangoni convection around the drops is reduced. Even water drops in the organic phase, e.g. in Fig. 8(b), showed periodic re-amplifications of Marangoni convection, since qualitatively the same conditions (vertical concentration gradient and initially stable density stratification) are present there due to the mass transfer of 2-propanol across the interface of the two-layer system.

Furthermore, to check the robustness and the mechanism of the relaxation oscillations, we also worked with bubbles in both the

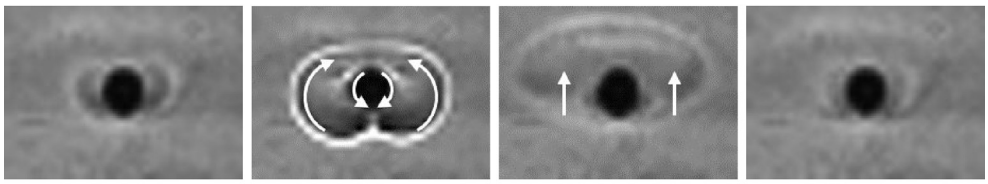

Fig. 6. Cycle of relaxation oscillation at a drop of paraffin oil immersed in the aqueous phase, see Fig. 4(a). White arrows indicate the direction of flow in the active ((a) and (b)) and relaxation phase ((c) and (d)). The width of the shown window is 2.4 mm.

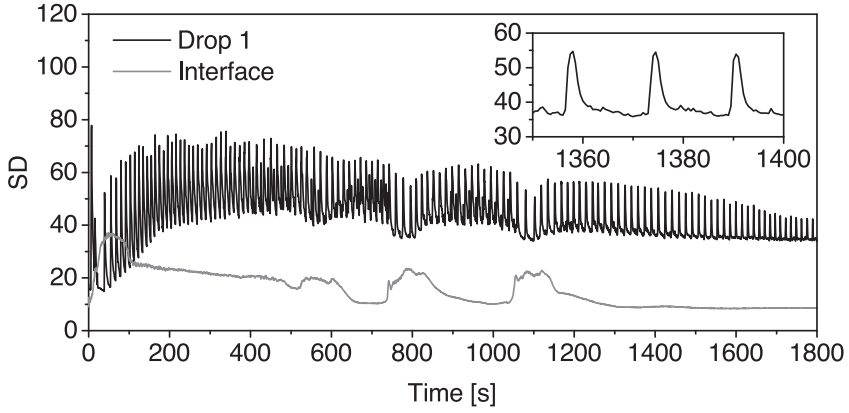

Fig. 7. Temporal evolution of standard deviation of gray value distribution for Drop 1, cf. Fig. 4(a), and the overlying interface of the two-layer system (gray curve). The inset details three periods of relaxation oscillations at Drop 1.

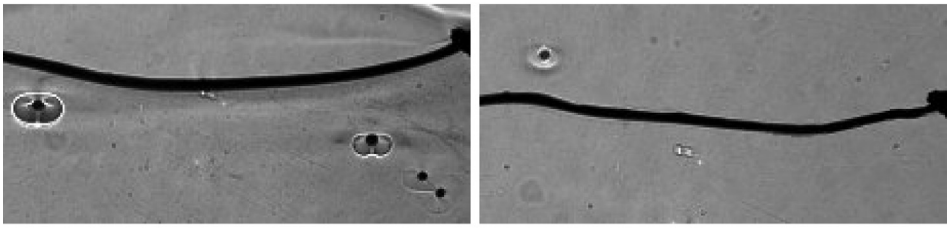

Fig. 8. Active stage of relaxation oscillations for different drops. The width of the shown window is 15 mm.

aqueous phase (Fig. 9(a)) and the organic phase (Fig. 9(b)). The bubble in (b) sits under the cover glass of the narrow cuvette, i.e. it is observed in top view. In the aqueous phase, a bubble was inserted at the tip of a capillary to prevent its immediate rise due to buoyancy forces. Both bubbles show the same type of relaxation oscillations as the drops; the circular fronts around the bubbles are their fingerprint. Contrary to the drops, it is obviously justified to neglect mass transfer into or from the air bubble. Hence it can be conjectured that mass transfer into or from the drops might as well play a minor effect. This is substantiated by the fact that the volume of the drops is very small, so their interior is equilibrated quickly.

On analyzing the frequency of relaxation oscillations for the two liquid configurations of water and paraffin oil, it turns out that the frequency is roughly by a factor of ten lower if the surrounding phase is paraffin oil instead of water. This difference, which was observed both for drops and bubbles, is attributed to the higher viscosity of paraffin oil leading to both slower convection and diffusion. Furthermore, the magnitude of density change per 2-propanol concentration in paraffin oil is approx. three times lower compared to the aqueous solution, cf. Table 1.

To sum up, the most probable mechanism of the relaxation oscillations is the consumption and regeneration of the vertical concentration gradient. However, from former works (cf. overview in Section 1) it is known that strong surfactants can also lead to

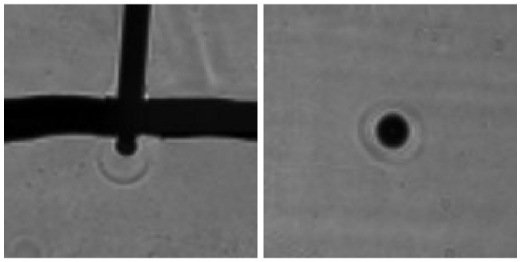

Fig. 9. Active stage of relaxation oscillations for different bubbles. The size of the shown window is 5 mm × 5 mm. The relaxation oscillations at bubble (a) are detailed in Fig. 12(b).

a periodic breakdown of Marangoni convection. Even though a simple alcohol was chosen as the surface-active solute, the effect of adsorption/desorption kinetics might not be excluded a priori. Furthermore, the experiments were found to be quite sensitive to impurities (cf. Section 2.1) which act similar to surfactants, adsorbing at the interface. Therefore, simulations were performed in order to rule out the influence of adsorption/desorption kinetics as the

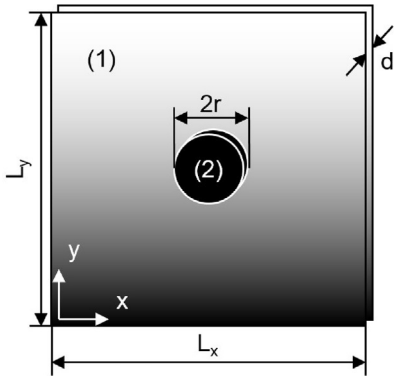

Fig. 10. Sketch (not drawn to scale) of the model geometry to simulate convection at a drop/bubble (2) placed in the aqueous phase (1).

primary cause for the breakdown of Marangoni convection in our experiments. As detailed below, a simplified model is considered which contains all relevant ingredients to describe the physics of the mechanism proposed in this section.

4. Simulations

4.1. Mathematical model

We use a diffuse interface model to simulate the two-phase flow problem with a surface-active solute. Assuming a parabolic velocity profile between the plates of the Hele-Shaw cell allows us to consider the flow equations in 2D by introducing an additional friction term depending on the Hele-Shaw gap width d [49–52,48]. As shown in Fig. 10, the drop/bubble is modeled as a cylindrical fluid domain between the plates to allow 2D computations. In the surrounding aqueous phase, an initially constant vertical concentration gradient of 2-propanol is supposed, whereas the solute concentration in the drop is neglected ($c^{(2)} = 0$). A phase field ϕ is used to represent the phases, with $\phi = 0$ in the drop and $\phi = 1$ in the surrounding fluid. We assume diffusion-limited adsorption where local thermodynamic equilibrium exists between the excess concentration Γ at the interface and the solute concentration $c = c^{(1)}$ adjacent to the interface. A linear relation between both quantities $\Gamma = Kc$ (Henry's model) is applied so that interfacial tension as well depends linearly on c (cf. Eq. 2). Hence, the concentration of the surface-active solute enters our model solely in terms of c. The mass transport is modelled by an advection-diffusion equation and the momentum transport by the incompressible Navier–Stokes equations coupled with the shear stress balance at the interface. We validated numerically that the inertia term in the Navier–Stokes equations can be omitted in the considered parameter regime.

The resulting governing equations for velocity $\mathbf{v}$, pressure p and surfactant concentration c in the aqueous phase are based on [53]:

$$\rho(\phi, c)\partial_t \mathbf{v} - \nabla\cdot(\eta(\phi)(\nabla\mathbf{v} + \nabla\mathbf{v}^T)) + \frac{3}{d^2}\eta(\phi)\mathbf{v} + \nabla p + k\nabla\phi\otimes\nabla\phi\cdot\mathbf{v} = \mathbf{g}\rho(\phi, c) + \sigma_{ref}\alpha_c|\nabla\phi|\mathbf{P}\nabla c,$$

$$\nabla\cdot\mathbf{v} = 0,$$

$$\phi\partial_t c + \phi\mathbf{v}\cdot\nabla c - D^{(1)}\nabla\cdot(\phi\nabla c) - D_n\nabla\cdot(\mathbf{n}\cdot\nabla c\,|\nabla\phi|\,\mathbf{n}) = 0,$$

where $\mathbf{g}$ is the gravitational acceleration, $\mathbf{P} = \mathbf{I} - \mathbf{n}\otimes\mathbf{n}$ is the surface projection, $\mathbf{I}$ is the identity matrix and $\mathbf{n} = \nabla\phi/|\nabla\phi|$ is the outer normal to the drop. Linear interpolations are used for the density $\rho(\phi, c) = \phi\rho_{ref}^{(1)}(1 - \beta_c^{(1)}c) + (1-\phi)(\rho_{ref}^{(2)}(1 - \beta_c^{(2)}c))$ and viscosity $\eta(\phi) = \phi(\eta^{(1)}) + (1-\phi)\eta^{(2)}$. Note that the positive semi-definite operator $k\nabla\phi\otimes\nabla\phi\cdot\mathbf{v}$ with penalty constant $k = 1$ kg/ms, enforces zero normal velocity at the drop surface, as can be shown using matched asymptotic analysis [54]. This mimics the experimentally observed immobility of the drop whose pinning at the wall of the Hele-Shaw cell counteracts gravity. Further, D_n is an interfacial normal diffusion ensuring the desired no flux boundary condition $\mathbf{n}\cdot\nabla c = 0$ at the drop surface. For the definition of the remaining quantities we refer to Tables 1 and 2.

Simulations were performed for two different sets of material parameters corresponding to an aqueous solution of 2-propanol surrounding a paraffin oil drop (Table 1) or an air bubble (Table 2). The drop and bubble diameter $2r = 0.3$ mm matches the size of Drop 1 in Section 3.3. For the diffusive mass transfer between two infinitely extended phases, an analytical solution exists [55]. Applying this solution to the diffusive mass transfer of 5 vol% 2-propanol between paraffin oil and water, the concentration gradient in the aqueous phase at a time of 600 s and a distance to the interface of 1 mm was calculated to $\frac{dc}{dy} := 25.4$ mol/(l·m). The distance of 1 mm again was chosen according to the position of Drop 1 with respect to the overlying interface. The time of 600 s approximately corresponds to the maximum concentration gradient of the diffusive solution at the location of the drop. This value therefore should be sufficient to trigger Marangoni convection as observed in the experiments. Hence, for the concentration field we use $c = \frac{dc}{dy}y$ as initial and boundary condition, with y being the vertical coordinate. For the velocity, the initial and boundary condition is set to $\mathbf{v} = 0$. This quiescent initial state is unstable, since the vertical concentration gradient imposes interfacial tension gradients at the drop surface and Marangoni convection sets in as detailed below. The domain size was chosen $L_x \times L_y = 8$ mm $\times$ 8 mm which was verified to be large enough to eliminate finite-size effects. For details on discretization and implementation we use the same procedure as for similar two-phase models with interfacial particles and refer to [56].

4.2. Numerical results

The simulations are in fact able to reproduce a periodic breakdown and re-amplification of Marangoni convection. Fig. 11 shows two snapshots of the concentration distribution around the drop for the stage of active Marangoni convection (a) and the end of the relaxation stage (b), roughly corresponding to Fig. 6(b) and (d) in the experiments, respectively. The observed structure of the concentration distribution agrees with the mechanism proposed in Section 3.3. In the active stage (Fig. 11(a)), the strong inflow of solute-rich fluid at the top of the drop is visible along with the mixing zone surrounding the drop. The isolines of concentration virtually enclose the drop as the concentration gradient is gradually reduced. Finally, due to the homogeneous concentration distribution at the drop surface, the gradients in interfacial tension are exhausted and interfacial convection breaks down. Only weak Marangoni flow takes place in the subsequent relaxation stage, accompanied by diffusion and buoyant convection in the aqueous phase. At the end of the relaxation stage (Fig. 11(b)), the isolines again take a more horizontal shape, indicating the restoration of the vertical concentration gradient. This means that sufficient Marangoni driving force is available to amplify the interfacial flow and the next cycle of active convection is initiated.

To characterize the evolution of the relaxation oscillations, the mean solute concentration $1/(2\pi r)\int_\Omega|\nabla\phi|c\,d\mathbf{x}$ at the drop/bubble surface Ω is shown in Fig. 12(a) as a function of time for a drop (black curve) and an air bubble (gray curve). In the inflow zone of

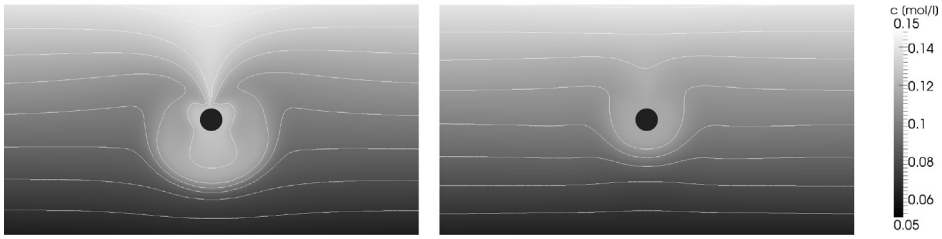

(a) Active stage of Marangoni convection corresponding to the local maximum in Fig. 12(a) at t = 57 s

(b) End of relaxation stage corresponding to the local minimum in Fig. 12(a) at t = 103 s

Fig. 11. Concentration distribution from simulations of a paraffin oil drop placed in an aqueous solution with a vertical gradient of 2-propanol. Shown is a section of 5.5 mm × 3 mm of the computational domain.

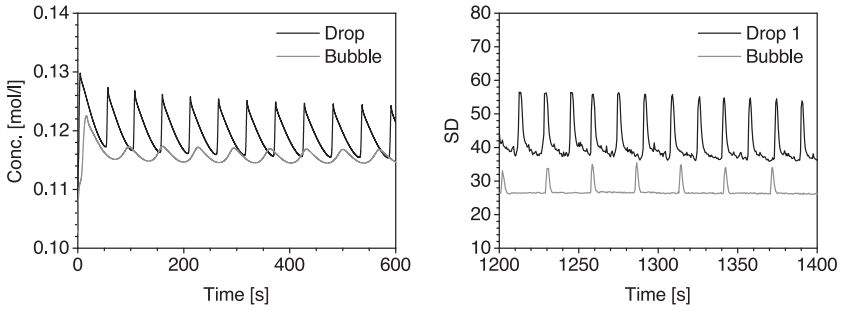

(a) Simulation

(b) Experiment

Fig. 12. Relaxation oscillations for a drop of paraffin oil resp. an air bubble placed in an aqueous solution of 2-propanol. Numerical results in (a) show the mean solute concentration at the drop/bubble surface, experimental results in (b) show the standard deviation of gray value distribution. The experimental results are for Drop 1 (cf. Fig. 7) and the bubble in Fig. 9(a).

Marangoni convection, solute-rich fluid is sucked to the drop surface, thereby increasing the concentration at the interface. Since the initial concentration gradient is constant throughout the whole domain, the first cycle is most intense, while the subsequent periods start from a pre-mixed state. In the quiet relaxation phase, the concentration at the interface drops again. As in the experiments, this process repeats in many cycles. The experimental results are plotted again in Fig. 12(b) for direct comparison. Note, that for accessibility reasons different quantities are displayed for the numerical and experimental results, i.e. the mean solute concentration at the drop/bubble surface is shown vs. the standard deviation of the shadowgraph gray value distribution. Therefore, the shape of the oscillations differs to a certain extent in Fig. 12((a) and (b)). The temporal domain of (b) is in the later stage of the experiment, where the convection around the drop/bubble is no longer influenced by the Marangoni convection at the overlying interface of the two-layer system. Qualitative agreement can be found between the relaxation oscillations in the experiments and simulations. Both the frequency and amplitude of the oscillations are lower for the simulation of an air bubble compared to those of the drop in Fig. 12(a). The same is observed in the experiments (b), where the less intense convection around the air bubble yields a lower contrast for the concentration front of the mixed zone (see Fig. 9(a)). However, an additional influence of the capillary can be expected for the experimental air bubble. The capillary probably alters the inflow of solute-rich fluid at the top of the bubble to a certain extent. The order of magnitude obtained for the oscillation frequency in the simulations is satisfactory considering the simplifications inherent in the theoretical model (cf. Section 4.1). Besides the applied linearizations for the dependence of interfacial/surface tension and solution density on 2-propanol concentration, and general uncertainties in the material properties, the 2D Hele-Shaw approximation is the main source for the deviations observed. Since the size of the drop (0.3 mm) is significantly smaller than the gap width of the Hele-Shaw cell (1 mm), only one side of the drop touches the wall in the experiments whereas the Hele-Shaw approximation assumes a cylindrical form of the drop between the glass plates. Therefore, significant 3D effects have to be taken into account, which certainly influence the temporal evolution. Our theoretical approach however appears sufficient to generally check the occurrence of relaxation oscillations on basis of the proposed mechanism, with the advantage of a strongly reduced computational cost compared to full 3D simulations.

5. Discussion and conclusion

The numerical simulations show that adsorption/desorption kinetics of the surface-active solute are not the main cause for the observed relaxation oscillations, since the underlying model disregards surfactant accumulation at the interface and introduces Marangoni effects in terms of the solute concentration adjacent to the interface. Surely more refined models taking into account nonlinear adsorption isotherms likewise would be able to reproduce the relaxation oscillations. However, the applied linear model, which is commonly used for weakly surface-active solutes, underlines that the bulk mixing effect by the Marangoni convection is the main reason for the termination of the active stage in our system compared to effects of adsorption/desorption kinetics.

Furthermore, the simulations corroborate the conclusion drawn from the experiments with bubbles that mass transfer into or from the drops is not the determining factor. The interplay between Marangoni convection in the active phase and diffusion accompanied by buoyant convection in the relaxation phase is identified via experimental shadowgraph images. These observations are supported by the simulations. Therefore, the proposed mechanism

based on the consumption and regeneration of the vertical concentration gradient in the vicinity of the drops can be regarded as valid.

However, the evolution appearing at the drops is not only interesting as a stand-alone phenomenon. The universal occurrence of the relaxation oscillations for various drops and bubbles in the system paraffin oil/2-propanol/water suggests that an analogous mechanism affects the periodic decay and re-amplification of Marangoni convection in 2-layer systems with interfacial curvature. As the drops provide both a defined curvature and strong geometrical constraints on the length scale of Marangoni convection, the temporal periodicity takes a markedly regular form compared to the two-layer system in the cuvettes or the Hele-Shaw cell. Nevertheless, the necessary conditions of geometrical confinement, intense mixing by Marangoni convection and facilitated instability by interfacial curvature is also present in our two-layer system. This argumentation is supported by the lack of periodicity if the interface is sufficiently planar, cf. Section 3.2. In the case of a perfectly planar interface, diffusion would have to rebuild the vertical concentration gradient along the whole mixing zone until another convection cycle can set in via the instability mechanism. This was not observed within the time frame of our experiments as the characteristic time of diffusion in the donating phase $\tau_d \sim (l_{mix}^{(2)})^2/D^{(2)}$ over the height of the mixing zone $l_{mix}^{(2)}$ is on the order of several hours. In the case of pronounced interfacial curvature, gradients in interfacial tension are easily rebuilt, since the upper parts of the interface virtually protrude from the mixing zone. Hence, a pronounced interfacial curvature is considered as a determining factor for periodically arising Marangoni convection in systems with a simple surface-active solute. This is not restricted to our system paraffin oil/2-propanol/water, but might also apply to other liquids if the capillary length κ is not too small compared to the geometrical dimensions of the two-layer interface.

The strikingly regular relaxation oscillations at drops and bubbles are an attractive phenomenon which deserves further study. Besides specific insights on how, for example, the shape of the relaxation oscillations depends on the material parameters, much can be learned about the nature of this oscillation type in fluidic systems based on simple droplet studies.

Acknowledgements

Financial support by the Deutsche Forschungsgemeinschaft in the framework of Priority Program 1506 is gratefully acknowledged (Grant Nos. Ec201/2, K.E. and Al1705/1, S.A.). Furthermore, we thank T. Köllner, T. Boeck, R. Miller, X. Yang and H. Linde for fruitful discussions and comments. Simulations were carried out at ZIH at TU Dresden.

References

[1] T. Sherwood, J. Wei, Interfacial phenomena in liquid extraction, Ind. Eng. Chem. 49 (1957) 1030–1034.
[2] Z.-S. Mao, J. Chen, Numerical simulation of the Marangoni effect on mass transfer to single slowly moving drops in the liquid–liquid system, Chem. Eng. Sci. 59 (2004) 1815–1828.
[3] M. Wegener, T. Eppinger, K. Bäumler, M. Kraume, A. Paschedag, E. Bänsch, Transient rise velocity and mass transfer of a single drop with interfacial instabilities – numerical investigations, Chem. Eng. Sci. 64 (2009) 4835–4845.
[4] J. Wang, Z. Wang, P. Lu, C. Yang, Z.-S. Mao, Numerical simulation of the Marangoni effect on transient mass transfer from single moving deformable drops, AIChE J. 57 (2011) 2670–2683.
[5] R.F. Engberg, M. Wegener, E.Y. Kenig, The impact of Marangoni convection on fluid dynamics and mass transfer at deformable single rising droplets – a numerical study, Chem. Eng. Sci. 116 (2014) 208–222.
[6] W. Han, Z. Lin, Learning from coffee rings: ordered structures enabled by controlled evaporative self-assembly, Angew. Chem. Int. Ed. 51 (2012) 1534–1546.
[7] S.-M. Kang, S. Hwang, S.-H. Jin, C.-H. Choi, J. Kim, B.J. Park, D. Lee, C.-S. Lee, A rapid one-step fabrication of patternable superhydrophobic surfaces driven by Marangoni instability, Langmuir 30 (2014) 2828–2834.
[8] C.V. Sternling, L.E. Scriven, Interfacial turbulence: hydrodynamic instability and the Marangoni effect, AIChE J. 5 (1959) 514–523.
[9] M. Hennenberg, T.S. Sørensen, A. Sanfeld, Deformational instability of a plane interface with transfer of matter. Part 1. Non-oscillatory critical states with a linear concentration profile, Journal of the Chemical Society, Farad. Trans. 2: Mol. Chem. Phys. 73 (1977) 48–66.
[10] S. Slavtchev, M. Hennenberg, J.-C. Legros, G. Lebon, Stationary solutal Marangoni instability in a two-layer system, J. Colloid. Interface Sci. 203 (1998) 354–368.
[11] S. Slavtchev, P. Kalitzova-Kurteva, M. Mendes, Marangoni instability of liquid–liquid systems with a surface-active solute, Colloid. Surf. A: Physicochem. Eng. Aspects 282–283 (2006) 37–49.
[12] K. Schwarzenberger, T. Köllner, H. Linde, T. Boeck, S. Odenbach, K. Eckert, Pattern formation and mass transfer under stationary solutal Marangoni instability, Adv. Colloid Interface Sci. 206 (2014) 344–371.
[13] S. Chen, B. Fu, X. Yuan, H. Zhang, W. Chen, K. Yu, Lattice Boltzmann method for simulation of solutal interfacial convection in gas-liquid system, Ind. Eng. Chem. Res. 51 (2012) 10955–10967.
[14] A. Javadi, M. Karbaschi, D. Bastani, J. Ferri, V. Kovalchuk, N. Kovalchuk, K. Javadi, R. Miller, Marangoni instabilities for convective mobile interfaces during drop exchange: experimental study and CFD simulation, Colloid. Surf. A: Physicochem. Eng. Aspects 441 (2014) 846–854.
[15] T. Köllner, K. Schwarzenberger, K. Eckert, T. Boeck, Multiscale structures in solutal Marangoni convection: three-dimensional simulations and supporting experiments, Phys. Fluids 25 (2013) 092109.
[16] C.A.P. Bakker, P.M. van Buytenen, W.J. Beek, Interfacial phenomena and mass transfer, Chem. Eng. Sci. 21 (1966) 1039–1046.
[17] J.C. Berg, C.R. Morig, Density effects in interfacial convection, Chem. Eng. Sci. 24 (1969) 937–946.
[18] D. Lavabre, V. Pradines, J.-C. Micheau, V. Pimienta, Periodic Marangoni instability in surfactant (CTAB) liquid/liquid mass transfer, J. Phys. Chem. B 109 (2005) 7582–7586.
[19] N.M. Kovalchuk, D. Vollhardt, Oscillation of interfacial tension produced by transfer of nonionic surfactant through the liquid/liquid interface, J. Phys. Chem. C 112 (2008) 9016–9022.
[20] R. Tadmouri, N. Kovalchuk, V. Pimienta, D. Vollhardt, J.-C. Micheau, Transfer of oxyethylated alcohols through water/heptane interface: transition from non-oscillatory to oscillatory behaviour, Colloid. Surf. A: Physicochem. Eng. Aspects 354 (2010) 134–142.
[21] H. Linde, Zur Kinetik des Stoffüberganges über die Grenzfläche zweier flüssiger Phasen, Monatsberichte der Deutschen Akademie der Wissenschaften zu Berlin 1, 1959, pp. 586–595.
[22] N. Kovalchuk, D. Vollhardt, Marangoni instability and spontaneous non-linear oscillations produced by liquid interfaces by surfactant transfer, Adv. Colloid Interface Sci. 120 (2006) 1–31.
[23] N. Kovalchuk, D. Vollhardt, Spontaneous nonlinear oscillation produced by alcohol transfer through water/alkane interface: an experimental study, Colloid. Surf. A: Physicochem. Eng. Aspects 291 (2006) 101–109.
[24] N.M. Kovalchuk, D. Vollhardt, Effect of buoyancy on appearance and characteristics of surface tension repeated auto-oscillations, J. Phys. Chem. B 109 (2005) 15037–15047.
[25] H. Linde, P. Schwartz, H. Wilke, Dissipative structures and nonlinear kinetics of the Marangoni-instability, in: Dynamics and Instability of Fluid Interfaces, Springer, 1979, pp. 75–119.
[26] K. Kostarev, A. Shmyrov, A. Zuev, A. Viviani, Convective and diffusive surfactant transfer in multiphase liquid systems, Exp. Fluids 51 (2011) 457–470.
[27] M. Lappa, C. Piccolo, L. Carotenuto, Fluid dynamics and dissolution kinetics in immiscible organic systems with dispersed droplets, Colloid. Surf. A: Physicochem. Eng. Aspects 261 (2005) 177–186.
[28] E. Schwarz, Zum Auftreten von Marangoni-Instabilität, Wärme- und Stoffübertragung 3 (1970) 131–133.
[29] E. Nakache, M. Dupeyrat, M. Vignes-Adler, The contribution of chemistry to new Marangoni mass-transfer instabilities at the oil/water interface, Farad. Discuss. Chem. Soc. 77 (1984) 189–196.
[30] A. Shioi, H. Kumagai, Y. Sugiura, Y. Kitayama, Oscillation of interfacial tension and spontaneous interfacial flow at a water/oil interface composed of di(2-ethylhexyl)phosphoric acid, Langmuir 18 (2002) 5516–5522.
[31] Y. Ikezoe, S. Ishizaki, T. Takahashi, H. Yui, M. Fujinami, T. Sawada, Hydrodynamically induced chemical oscillation at a water/nitrobenzene interface, J. Colloid Interface Sci. 275 (2004) 298–304.
[32] R. Sczech, K. Eckert, M. Acker, Convective instability in a liquid–liquid system due to complexation with a crown ether, J. Phys. Chem. A 112 (2008) 7357–7364.
[33] T. Miyaoka, J. Nishimura, Y. Iida, S. Maki, A. Shioi, Ion-selective Marangoni instability-chemical sensing of specific cation for macroscopic movement, Chaos: Interdiscip. J. Nonlinear Sci. 22 (2012) 037111.
[34] K. Schwarzenberger, K. Eckert, S. Odenbach, Relaxation oscillations between Marangoni cells and double diffusive fingers in a reactive liquid–liquid system, Chem. Eng. Sci. 68 (2012) 530–540.
[35] K. Eckert, M. Acker, R. Tadmouri, V. Pimienta, Chemo-Marangoni convection driven by an interfacial reaction: pattern formation and kinetics, Chaos: Interdiscip. J. Nonlinear Sci. 22 (2012) 037112.
[36] D. Lide, CRC Handbook of Chemistry and Physics: A Ready-reference Book of Chemical and Physical Data, CRC Press, 2004.
[37] Carl Roth GmbH & Co. KG, Specification of paraffin oil, Ph.Eur., DAB, low viscosity.

[38] G.W. Paul, L.E.M. De Chazal, Interfacial tensions in ternary liquid–liquid systems, J. Chem. Eng. Data 12 (1967) 105–107.
[39] W. Hayduk, H. Laudie, Prediction of diffusion coefficients for nonelectrolytes in dilute aqueous solutions, AIChE J. 20 (1974) 611–615.
[40] J. Li, P.W. Carr, Accuracy of empirical correlations for estimating diffusion coefficients in aqueous organic mixtures, Anal. Chem. 69 (1997) 2530–2536.
[41] H. Iwata, K. Shimada, Formulas, Ingredients and Production of Cosmetics: Technology of Skin- and Hair-Care Products in Japan, Springer, Japan, 2012.
[42] A. Mizev, Influence of an adsorption layer on the structure and stability of surface tension driven flows, Phys. Fluids 17 (2005) 122107.
[43] G. Vazquez, E. Alvarez, J.M. Navaza, Surface tension of alcohol + water from 20 to 50 °C, J. Chem. Eng. Data 40 (1995) 611–614.
[44] Y. Shi, K. Eckert, A novel Hele-Shaw cell design for the analysis of hydrodynamic instabilities in liquid–liquid systems, Chem. Eng. Sci. 63 (2008) 3560–3563.
[45] C. Almarcha, Y. R'Honi, Y. De Decker, P.M.J. Trevelyan, K. Eckert, A. De Wit, Convective mixing induced by acid-base reactions, J. Phys. Chem. B 115 (2011) 9739–9744.
[46] M.A. Budroni, L.A. Riolfo, L. Lemaigre, F. Rossi, M. Rustici, A. De Wit, Chemical control of hydrodynamic instabilities in partially miscible two-layer systems, J. Phys. Chem. Lett. 5 (2014) 875–881.
[47] P.-G. De Gennes, F. Brochard-Wyart, D. Quéré, Capillarity and wetting phenomena: drops, bubbles, pearls, waves, Springer, 2004.
[48] T. Köllner, K. Schwarzenberger, K. Eckert, T. Boeck, Solutal Marangoni convection in a Hele-Shaw geometry: impact of orientation and gap width, Eur. Phys. J. Spec. Topics 224 (2015) 261–276.
[49] W. Boos, A. Thess, Thermocapillary flow in a Hele-Shaw cell, J. Fluid Mech. 352 (1997) 305–330.
[50] D. Bratsun, A. De Wit, On Marangoni convective patterns driven by an exothermic chemical reaction in two-layer systems, Phys. Fluids 16 (2004) 1082–1096.
[51] A. Grahn, Two-dimensional numerical simulations of Marangoni-Bénard instabilities during liquid–liquid mass transfer in a vertical gap, Chem. Eng. Sci. 61 (2006) 3586–3592.
[52] D. Bratsun, A. De Wit, Buoyancy-driven pattern formation in reactive immiscible two-layer systems, Chem. Eng. Sci. 66 (2011) 5723–5734.
[53] K.E. Teigen, P. Song, J. Lowengrub, A. Voigt, A diffuse-interface method for two-phase flows with soluble surfactants, J. Comput. Phys. 230 (2011) 375–393.
[54] X. Li, J. Lowengrub, A. Rätz, A. Voigt, Solving PDEs in complex geometries: a diffuse domain approach, Commun. Math. Sci. 7 (2009) 81–107.
[55] J. Crank, The Mathematics of Diffusion, Clarendon, Oxford, 1975.
[56] S. Aland, J. Lowengrub, A. Voigt, A continuum model of colloid-stabilized interfaces, Phys. Fluids 23 (2011) 062103.